Earth Planet. Sci. Lett. 629 (2024) 118600

Contents lists available at ScienceDirect

Earth and Planetary Science Letters

journal homepage: www.elsevier.com/locate/epsl

Rapid removal and replacement of dissolved organic matter during circulation through ultramafic crust

Susan Q. Lang [a,*], Bryan Benitez-Nelson [b], Malayika Vincent [b], Ronald Soong [c], Flavio V. C. Kock [c], Daniel H. Lysak [c], Amy Jenne [c], André J. Simpson [c]

[a] Department of Geology and Geophysics, Woods Hole Oceanographic Institution, Woods Hole, MA 02543, USA
[b] School of the Earth, Ocean and Environment, University of South Carolina, Columbia, SC 29169, USA
[c] Environmental NMR Center, University of Toronto Scarborough, Toronto, Ontario M1C1A4, Canada

ARTICLE INFO

Editor: Dr L Coogan

Keywords:
Serpentinization
Dissolved organic carbon
Radiocarbon
Nuclear magnetic resonance
Hydrothermal

ABSTRACT

Large volumes of seawater have passed through the rocky subseafloor throughout Earth's history. The scale of circulation is sufficiently large to impact the cycling of marine dissolved organic carbon (DOC), one of the largest pools of reduced carbon on Earth whose sources and sinks remain enigmatic, and to sequester carbon over geologic timescales. While the fate of DOC in numerous mafic systems has been examined, no previous reports are available on the less studied but still abundant ultramafic systems. We analyzed the concentration and composition of DOC from the Lost City hydrothermal field (30°N, Mid-Atlantic Ridge), a long-lived ultramafic system with minimal magmatic input. We show that per liter of seawater, more DOC is removed and a rate >650 times faster rate than in mafic ridge flank systems. Simultaneously, newly synthesized ^{14}C-free organics are exported into the water column, adding a pre-aged component to the deep DOC pool. The sequestration of oceanic organic molecules onto minerals could partially account for the substantial total organic carbon present in ultramafic rocks, which is currently interpreted as evidence of chemoautotrophy or abiotic synthesis.

1. Introduction

Carbon compounds carried with downwelling seawater into the oceanic crust are subjected to elevated temperatures, redox changes, interactions with mineral surfaces, and, since the emergence of life, modification by microbial communities during circulation through the rocky subseafloor. Organic molecules also form in the absence of life when appropriate catalysts and geochemical conditions are available (Foustoukos and Seyfried, 2004; McCollom and Seewald, 2007; Lang et al., 2012; McDermott et al., 2015), raising the possibility that such environments may have played an important role in early biochemical evolution (Martin and Russell, 2007). Determining the fate of carbon as fluids pass through the crust therefore provides constraints on global fluxes and predictive insights into the environmental conditions conducive to hosting subseafloor life or abiotic synthesis on Earth and other planetary bodies.

The starting fluid for submarine hydrothermal systems is deep seawater that, in modern oceans, contains dissolved organic carbon (DOC) largely derived from biological activity in the upper photic zone. The deep ocean is dominated by refractory DOC (RDOC), an extremely long-lived suite of molecules able to persist thousands of years through multiple thermohaline circulation cycles (Hansell, 2013).

The loss of seawater RDOC during hydrothermal circulation has been demonstrated at multiple types of mafic systems hosted on basaltic and gabbroic rocks (see Lang, in press, for review). The DOC concentration of fluids in axial high temperature black smoker fluids and through warm and cool ridge flanks are up to 70% lower than deep seawater (Lang et al., 2006; McCarthy et al., 2011; Lin et al., 2012; Shah Walter et al., 2018; Longnecker et al., 2018). The largest fluid flux occurs through cool ridge flank systems, which could account for a loss of 5% of the RDOC loss in the deep ocean (Shah Walter et al., 2018).

Ultramafic systems differ from these environments formed by magmatic processes. They occur when deep mantle rocks are uplifted and exposed to seawater triggering serpentinization, a series of hydration reactions that incorporates >10 wt% water into the rocks and produces iron-rich clays, magnetite, and other minerals (Frost and Beard, 2007; Evans, 2008). Ultramafic rocks account for 20–25% of the seafloor in slow spreading ridges (Cannat et al., 2010) and their

* Corresponding author.
E-mail address: sqlang@whoi.edu (S.Q. Lang).

https://doi.org/10.1016/j.epsl.2024.118600
Received 8 September 2023; Received in revised form 1 February 2024; Accepted 2 February 2024
Available online 14 February 2024
0012-821X/© 2024 Elsevier B.V. All rights reserved.

interaction with seawater has major consequences for long-term, global geochemical fluxes of H_2O, Cl, B, U, S, and inorganic C (Früh-Green et al., 2004).

Unlike mafic-hosted systems, the hydrothermal fluids that have interacted with ultramafic rocks have higher organic carbon concentrations than seawater (Lang et al., 2010; McDermott et al., 2015). Hydrogen (H_2) is a by-product of the serpentinization reaction and provides the thermodynamic drive for the synthesis of small organic molecules such as formate, methane, and short-chain hydrocarbons, which are produced abiotically in the subseafloor and exported in fluids (Proskurowski et al., 2008; Lang et al., 2010; McDermott et al., 2015). Microbial activity also contributes organics to the system in the form of amino acids, acetate, lipids, and dense biofilms (Bradley et al., 2009; Lang et al., 2010, 2013; Méhay et al., 2013). The substantial de novo synthesis of biological and nonbiological organics does not preclude the removal of deep seawater RDOC but could mask it.

We examined the concentrations and characteristics of DOC in fluids from the Lost City hydrothermal field (LCHF, 30°N, MAR; Fig. 1) to determine if the removal of RDOC during hydrothermal circulation is a ubiquitous process that occurs with different rock types, and to characterize composition and isotopic signatures of organics that are exported. Samples were collected from individual venting chimneys that spanned temperatures from 11 to 96 °C, and were analyzed for the ^{14}C and ^{13}C of DOC and the molecular-level concentrations of indicator components such as amino acids and organic acids (Tables 1-3; Suppl Material Table S1). The portion of these fluids that could be isolated by solid phase extraction (SPE), which preferentially recovers the larger and less polar material that makes up RDOC over the small polar organics that dominate the Lost City fluids, were also analyzed by Nuclear Magnetic Resonance (NMR) and isotope ratio mass spectrometry (IRMS).

2. Methods

2.1. Sample collection and shipboard analyses

Hydrothermal fluids were collected in September 2018 during the AT42–01 expedition of the R/V Atlantis with the remotely operated

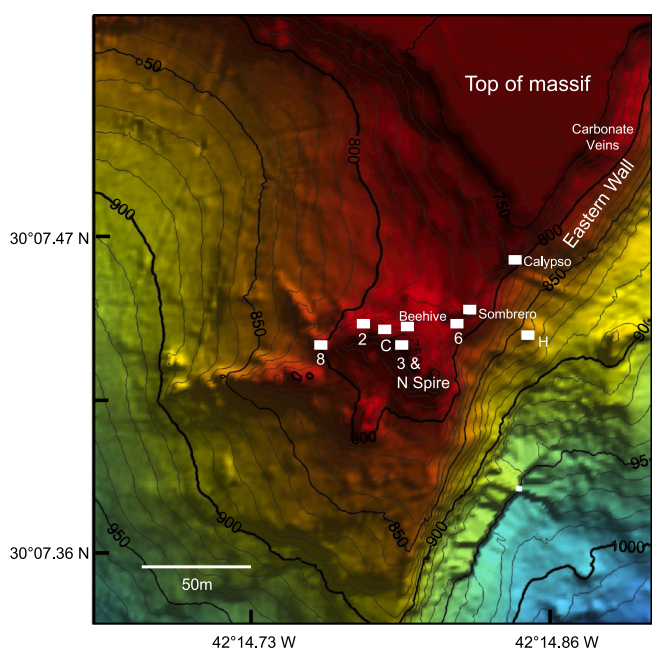

Fig. 1. Map of the Lost City hydrothermal field with the main focused flow locations identified with squares. Additional samples were collected from carbonate veins infilling seafloor fissures. Map modified from Kelley et al. (2005).

Table 1
Location, geochemical characteristics, and isotopic composition (^{13}C, ^{14}C) of DOC from Lost City fluids.

Sample Name	Location	Lat.	Long.	Depth (m)	Year	E.M. H_2 (mM)*	Mg^{2+} (mM)	Measured Values			Calculated hydrothermal endmember		
								DOC conc. (μM)	$\delta^{13}C_{DOC}$ (‰)	$F^{14}C_{DOC}$	DOC conc. (μM)	$\delta^{13}C_{DOC}$ (‰)	$F^{14}C_{DOC}$
J1110_C2	Marker C	30.1239	−42.1202	780	2018	8.2	11.1	64.5	−7.0	0.0922 ± 0.0023	70.6	−4.6	0.011 ± 0.005
J1108_C1	Marker B	30.1239	−42.1199	743	2018	9.6	1.9	72.6	−5.9	0.0457 ± 0.0033	73.7	−5.5	0.034 ± 0.003
J1107_C6	Marker 2	30.0744	−42.0722	764	2018	3.5	3.1	37.5	−4.1	0.0675 ± 0.0039	37.3	−2.9	0.030 ± 0.005
J1111_C3	Sombrero	30.1241	−42.1196	762	2018	11.3	21.8	62.0	−10.9	0.2548 ± 0.0024	76.2	−6.6	0.118 ± 0.010
J1111_C6	Vein on Wall	30.1244	−42.1187	864	2018	N.D.	36.6	39.2	N.D.	0.4630 ± 0.0042	34.0	N.D.	0.037 ± 0.083
J1110_C4	Marker 8	30.1237	−42.1207	801	2018	3.0	12.0	65.9	−5.9	0.2241 ± 0.0021	73.0	−3.1	0.159 ± 0.004
J1111_C5	Marker 3	30.1239	−42.1201	731	2018	11.2	13.4	68.4	−10.6	0.2956 ± 0.0029	77.5	−8.5	0.237 ± 0.005
AT42–01–007-V06-B10	Local Seawater	30° 2.5925′ N	42° 3.2708′ W	801	2018	N.D.	53.4	41.2	N.D.	0.6235 ± 0.0050	–	–	–
Atlantic SW***	Station A16N 66	57° 30.010′ N	19° 59.965′ W	875	2013	N.D.	–	42.2	−22.3	0.6181	–	–	–
Atlantic SW***	Station A22 26	32° 38.846′ N	64° 55.729′ W	1514	2012	N.D.	–	40.9	−22.1	0.6110	–	–	–

* Data from Aquino et al. (2022)
**Amino acid concentrations were not determined for AT42–01–007-V06-B10; the average results from two near-by CTD samples are reported.
*** Data from Druffel et al. (2016).

Table 2
Carbon content of Lost City fluids. N.D. is not determined and B.D.L. is below limit of detection.

Sample Name	Location	Avg. T (°C)	High T (°C)	Mg (mM/Kg)*	pH @ 22 °C*	DIC (mM)	DIC $\delta^{13}C$ (‰)	Formate (μM)	Acetate (μM)	THAA (nM)
J1108_C1	Marker Beehive	95.0	95.7	1.9	10.6	0.11	BDL	49.9	3.4	74
J1108_C2	Marker Beehive	95.3	95.4	0.9	10.8	0.07	BDL	N.D.	N.D.	N.D.
J1108_C3	Marker Beehive	95.4	95.6	0.4	10.8	0.05	BDL	50.0	3.5	131
J1108_C15	Marker Beehive	95.6	95.7	0.1	10.8	0.04	BDL	52.1	4.5	145
J1111_C4	Marker 3 (Camel Humps)	N.D.	85.0	26.6	9.0	1.14	0.9	24.9	1.5	302
J1111_C5	Marker 3 (Camel Humps)	N.D.	85.0	13.4	9.8	0.52	1.1	36.6	1.0	566
J1110_C1	Marker C	72.6	80.6	6.3	10.1	0.32	BDL	38.7	BDL	N.D.
J1110_C2	Marker C	78.4	80.0	11.1	10.0	0.50	0.9	35.8	2.3	211
J1110_C3	Marker C	74.7	79.6	9.3	10.0	0.40	0.6	37.6	3.7	221
J1110_C16	Marker C	74.7	79.7	5.9	10.1	0.24	BDL	N.D.	N.D.	N.D.
J1112_M1	Marker 6	N.D.	65.8	4.8	10.6	BDL	BDL	45.8	2.7	N.D.
J1107_C4	Marker 2	44.0	61.5	23.4	10.0	0.92	0.3	N.D.	N.D.	N.D.
J1107_C5	Marker 2	59.7	62.4	5.7	10.2	0.26	BDL	N.D.	N.D.	N.D.
J1107_C6	Marker 2	61.2	63.9	3.1	10.3	0.21	BDL	16.6	3.3	420
J1107_C7	Marker 2	46.8	58.3	21.8	10.1	0.68	−0.5	11.5	2.6	342
J1107_C2	Poseidon N. Spire	40.8	44.5	32.5	9.2	1.40	1.0	12.1	0.9	298
J1107_C3	Poseidon N. Spire	49.0	55.1	28.2	9.3	1.19	0.6	15.2	BDL	168
J1109_C3	Sombrero	N.D.	57.0	51.4	8.0	2.35	1.2	0.6	BDL	113
J1109_C5	Sombrero	N.D.	57.0	52.0	8.0	2.30	1.1	BDL	BDL	233
J1109_C6	Sombrero	N.D.	57.0	52.3	8.0	2.30	1.3	BDL	BDL	233
J1111_C1	Sombrero	48.2	56.8	25.2	9.1	1.04	0.9	27.8	1.0	N.D.
J1111_C2	Sombrero	49.0	56.7	24.1	9.2	0.99	0.9	30.4	4.3	119
J1111_C3	Sombrero	46.6	58.5	21.8	9.3	0.92	0.9	30.8	3.9	217
J1110_C4	Marker 8	46.7	53.8	12.0	10.0	0.28	BDL	8.3	6.2	238
J1110_C5	Marker 8	34.8	52.6	14.5	N.D.	0.39	−0.8	7.3	4.7	1405
J1108_C4	Calypso	24.6	26.2	36.3	9.2	1.60	1.0	N.D.	N.D.	N.D.
J1108_C5	Calypso	24.1	26.3	34.3	9.2	1.54	0.8	N.D.	N.D.	N.D.
J1108_C6	Calypso	28.0	31.8	35.3	9.2	1.64	1.0	BDL	3.7	70
J1108_C7	Calypso	31.7	32.9	31.4	9.3	1.37	0.9	BDL	2.2	111
J1108_C16	Calypso	29.7	31.8	33.3	9.3	1.53	0.9	BDL	4.2	85
J1109_C7	Vein on carbonate cap	N.D.	10.7	53.5	8.0	2.44	1.1	BDL	BDL	116
J1111_C6	Vein on Wall NE of Marker H	N.D.	22.0	36.6	9.1	1.59	0.9	BDL	BDL	61N.D.
J1109_C4	Seawater, 818 m	N.D.	N.D.	52.9	7.9	2.30	1.1	BDL	BDL	72
AT-4201–007-V06-B10	Seawater, 801 m	4	4	53.4	N.D.	N.D.	N.D.	N.D.	N.D.	101
AT-4201–001-V01-B3	Seawater, 1010 m	4	4	N.D.	N.D.	N.D.	N.D.	N.D.	N.D.	145

* Data from Aquino et al. (2022).

Table 3
Concentration and isotopic signature of solid phase extractable DOC (SPE-DOC). Multiple 1 L aliquots of each sample were extracted on separate cartridges and analyzed separately. The average and standard deviation of these replicates are reported. All aliquots from J1108_C15 and J1110_C16 constitute the Lost City central vent sample for NMR analysis, while all aliquots from J1111_C16 and J1108C16 constitute the Lost City peripheral vent sample.

Sample Name	Location	Highest Temp. (°C)	pH*	SPE-DOC (μM)	$\delta^{13}C_{DOC\text{-}SPE}$ (‰)	n
J1108_C15	Beehive	96	10.8	5.1 ± 2.7	−18.9 ± 1.2	3
J1110_C16	Marker C	81	10.3	11.0 ± 3.0	−18.1 ± 3.4	4
J1111_C16	Sombrero	62	9.1	18.1 ± 3.4	−20.3 ± 0.7	5
J1108_C16	Calypso	32	9.3	24.3 ± 2.4	−21.1 ± 0.3	7
AT42–22-CTD-02-B11	Seawater	4	7.7	26.9 ± 3.6	−22.2 ± 0.6	5

* data from Aquino et al. (2022).

vehicle (ROV) Jason II using the Hydrothermal Organic Geochemistry (HOG) sampler (Lang and Benitez-Nelson, 2021) (Table 1). Fluids were shunted through a titanium nozzle with an embedded temperature probe into acid washed (12 h with 10% trace metal grade HCl followed by 12 h with Milli-Q water and multiple rinses) Kynar® bags. Water column samples were collected using a Nisken Rosette.

Upon arrival on deck, aliquots for organic acid and amino acid concentrations were transferred to acid washed high density polyethylene bottles and frozen until later analysis. Samples for ^{14}C-DOC analysis were transferred directly from the Kynar® bags into amber glass bottles that had been previously muffled and stored in two sealed bags. Care was taken to prevent the containers or the bags contacting shipboard surfaces.

Five samples were subjected to SPE. They were pre-filtered through a muffled GF/75 filter (nominal pore size 0.3 μm) and acidified to a pH of 2 with trace metal grade HCl. SPE cartridges (Bond Elut PPL, 6 mL, Agilent P/N 12,255,002) were prepared by rinsing with methanol followed by Milli-Q water. Approximately 1 L of sample was then extracted per cartridge by passing it slowly over the phase (~0.5 mL/min) and the exact volume was recorded. For each sample, 3–5 cartridges were taken at each site. Cartridges were rinsed with 0.01 HCl to remove salt, dried with N_2. The sample was eluted with methanol, dried to a volume of 2 mL, and stored frozen.

2.2. Radiocarbon and stable carbon analysis of dissolved organic carbon

Frozen samples were analyzed by UV oxidation and Accelerator Mass Spectrometry (Beaupre et al., 2007; Xu et al., 2020) at the National Ocean Sciences Accelerator Mass Spectrometry facility.

2.3. Dissolved inorganic carbon (DIC and $\delta^{13}C_{DIC}$)

At sea, aliquots for dissolved inorganic carbon (DIC) were syringe filtered (0.2 μm) and injected into a Labco Exetainer® vial that had been previously spiked with 100 μL of phosphoric acid and flushed with helium. Samples were stored at room temperature until analysis by a GasBench II preparation device connected to a ConFlo IV interface and a Delta V Plus isotope ratio mass spectrometer (GasBench-IRMS, Thermo Fisher Scientific, Bremen, Germany). Two five point standard curves were prepared over a concentration range that bracketed the samples using lab standards (potassium bicarbonate, −38.1‰; lithium carbonate, −1.1‰) that had been previous calibrated to IAEA standards. The error of analysis was determined from external standards and the standard deviation of multiple injections to be 0.4 ‰. Samples with DIC concentrations below 0.35 mM generated peak sizes too small for accurate isotope measurements.

2.4. Organic acid concentrations

Organic acid concentrations (formate, acetate, propionate, pyruvate, butyrate, lactate) were analyzed by the method of Albert and Martens, 1997. An aliquot (1 mL) of each sample was spiked with 100 μL of pyridine buffer (1:1 mixture of Fisher TraceMetal grade 12 N HCl and pyridine) and purged with N_2. They were then spiked with 100 μL of 0.1 M 2-Nitrophenylhydrazine hydrochloride (Acros P/N 128,830,100) and 100 μL of 0.3 M 1-(3-Dimethylaminopropyl)−3-ethylcarbodiimide hydrochloride (Acros P/N 171,440,100) and reacted at room temperature overnight. They were then filtered (0.2 μm polyethersulfone) and analyzed immediately.

Derivatized samples were analyzed on a Thermo Ultimate 3000 UHPLC equipped with a Thermo Scientific Acclaim Organic Acid silica column (P/N 070,086, 3.0 × 150 mm, 3.0 μm diameter). Compounds were detected at 400 nm with a UV/Vis detector. Mobile phase A consisted of 2.5% n-Butanol, 25 mM sodium acetate, 2 mM tetrabutylammonium hydroxide 30-hydrate, and 50 mM tetradecyltrimethylammonium bromide, in Milli-Q water adjusted to pH of 4.5 with phosphoric acid. Mobile phase B was 100% Milli-Q water and mobile phase C was a 70:30 mixture of Methanol:Milli-Q water. The run started with 100% mobile phase A and ramped to 100% B over 49 min then 100% C at 59 min. The detection limit was 0.5 μM for each organic acid.

2.5. Amino acid concentrations

Samples were analyzed for total free amino acids (TFAA) and total hydrolizable amino acids (THAA). THAA samples were hydrolyzed by mixing 1:1 with 12 N Fisher TraceMetal grade with 1% 11 mM ascorbic acid that had been purged with N_2. Vials were purged with N_2 to remove oxygen, sealed, and reacted at 110 °C for 20 h. After hydrolysis, the samples were dried under N_2 to remove excess acid and redissolved in Milli-Q. This procedure was repeated until samples were neutral, at which point samples were derivatized with 2 mg mL-1 of o-Phthaldialdehyde (OPA) and 5 mg mL-1 of either N-isobutyryl-L-cystine (IBLC) or N-isobutyryl-D-cysteine (IBDC). Samples were analyzed separately with OPA/IBLC and OPA/IBDC to distinguish co-eluting peaks. Bovine serum albumin was analyzed as an external measure of hydrolysis induced racemization (Kaiser and Benner, 2005).

2.6. Solid phase extraction of dissolved organic carbon (SPE-DOC and $\delta^{13}C_{SPE\text{-}DOC}$)

For the analysis of $\delta^{13}C_{SPE\text{-}DOC}$, an aliquot (50 μL) of each 2 mL SPE cartridge extract was transferred to muffled Labco Exetainer® vial and dried under N2 to remove the methanol. They were then oxidized by adding 1 mL of saturated sodium persulfate solution (120 mM $Na_2S_2O_8$), purging the container with high purity helium and heating at 100 °C for 1 h to convert DOC to CO_2 (Lang et al., 2012). The isotopic signature of the evolved CO_2 was determined using a GasBench II preparation device connected to a ConFlo IV interface and a Delta V Plus isotope ratio mass spectrometer (GasBench-IRMS, Thermo Fisher Scientific, Bremen, Germany). Two five-point standard curves were prepared over a concentration range that bracketed the samples using lab standards (phthalic acid, −33.6 ‰; sucrose −12.4 ‰) that had been previous calibrated to IAEA standards.

2.7. Nuclear magnetic resonance (NMR) spectroscopy of SPE extracts

To obtain sufficient material for NMR analysis, the extracts from all SPE cartridges from a single sample were combined. Samples from locations with similar attributes were then further combined to obtain one 'Lost City Central' fluid (Beehive + Marker C), one 'Lost City Peripheral' fluid (Sombrero + Calypso), and one background seawater (Niskin cast above the Lost City field). The extracts were dried under N_2 to remove methanol and redissolved in ~3 mg of CD_3OD (99.96% purity, Sigma-Aldrich). All NMR experiments were performed and recorded on a Bruker Avance III spectrometer at 500.28 MHz (1H nucleus), equipped with a 1.7 mm, triple resonance (^1H, ^{13}C, ^{15}N) (TXI) Microprobe (Bruker, Fallanden, Switzerland) with an actively shielded Z-gradient at the University of Toronto. All channels were tuned and matched for each sample and the 90° pulses were calibrated on a per-sample basis, before data acquisition at room temperature (298°K). Standard ^1H NMR was performed using presaturation of the water signal with a 50 Hz RF field, 49,152 data points and an interscan delay which corresponded to 5 times the T1 (itself as measured on a per sample basis). Typically, the time between scans was ~8.8 s. Data were processed with a line broadening corresponding to 1 Hz in the transformed spectrum and a zero-filling factor 2.

Diffusion editing (Fig. S1) was performed using a bipolar pulse pair longitudinal encode-decode (BPPLED) sequence with encoding/decoding gradients of 2.5 ms at ~30 gauss cm-1 and a diffusion time of 200 ms. The diffusion edited spectra were processed with line broadening corresponding to 10 Hz in the transformed spectrum and a zero filling factor 2. The spectra were referenced to the lipid CH_2 peak at 1.29 ppm.

$^1H-^{13}C$ heteronuclear single-quantum coherence (HSQC) correlation experiments (Fig. S2) were collected in phase sensitive mode using Echo/Antiecho encoding and gradients for coherence selection and multiplicity editing (1/(2J(XH)) XH, XH3 positive, XH2 negative) during the selection step. 512 scans were collected for each of the 96 increments in the F1 dimension. 2048 time-domain points were recorded in the F2 dimension with a 1 J 1H-13C of 145 Hz. The F2 dimension was processed using an exponential function corresponding to a line broadening of 15 Hz and F1 using a sine-squared function with a π/2 phase shift and a zero-filling factor of 2. Spectral predictions were carried out using Advanced Chemistry Development's ACD/NMR Workbook using Neural Network Prediction algorithms (version 2021.2.2). Parameters used for prediction, including spectral resolution and base frequency, were chosen to match those of the real data sets as closely as possible.

2.8. Gas chromatography mass spectrometry of SPE extracts

After non-destructive NMR analysis, the SPE extracts were derivatized with N,O-bis(trimethylsilyl)trifluoro-acetamide (BSTFA + 10% TMS) at 60 °C for 30 min. The lipids were analyzed using an Agilent Technologies 5975 inert XL Mass Selective Detector after separation on an Agilent J&W GC HP-5MS UI capillary column (30 m x 0.25 mm i.d., 0.25 μm film thickness, P/N 19091S-433UIE) using helium as the carrier gas. Samples were injected in pulse splitless mode. The GC oven had an initial temperature of 70 °C, then was heated to 150 °C at 15 °C per min, then to 300 °C at 5 °C per min.

3. Results

3.1. Carbon geochemistry of fluids

The concentrations of DIC approach zero in the lowest Mg fluids (Fig. 2a, Table 2), consistent with it being largely absent in endmember fluids (Kelley et al., 2005; Proskurowski et al., 2008). The $\delta^{13}C_{DIC}$ of the hydrothermal fluids values were largely similar to local seawater, with the exception of Marker 8 and Marker 2 where it was somewhat more negative (Table 2). Formate (BDL – 52.1 μM) and acetate (BDL – 6.2 μM) were the only organic acids detected in the fluids. After correcting for entrainment of seawater during sampling by extrapolating to a zero-Mg endmember, the concentrations of formate were strongly positively associated with elevated H_2 concentrations (Fig. 3). A similar relationship between endmember acetate and H_2 concentrations was not present.

Amino acids in fluids from the main field had total concentrations of 70 – 1405 nM, compared to local deep seawater concentrations of 72 – 112 nM (Fig. 2b). The relative contributions from non-protein amino acids and D/L ratios are generally low (Table S1). No free amino acids were present above our detection limit of 5 nM.

3.2. Solid phase extracts of dissolved organic carbon (SPE-DOC)

The SPE-DOC concentrations of deep seawater contained 26.9 ± 3.6 μM with an isotopic composition of −22.2 ± 0.6 ‰ ($n = 5$, Table 3). The hottest collected fluids were from the Beehive vent and had SPE-DOC composition with 80% less carbon and more positive $\delta^{13}C_{SPE\text{-}DOC}$ values (5.1 ± 2.7 μM; −18.9 ± 1.2 ‰, $n = 3$). Cooler fluids had SPE-DOC compositions between these two endmember values (Fig. 4).

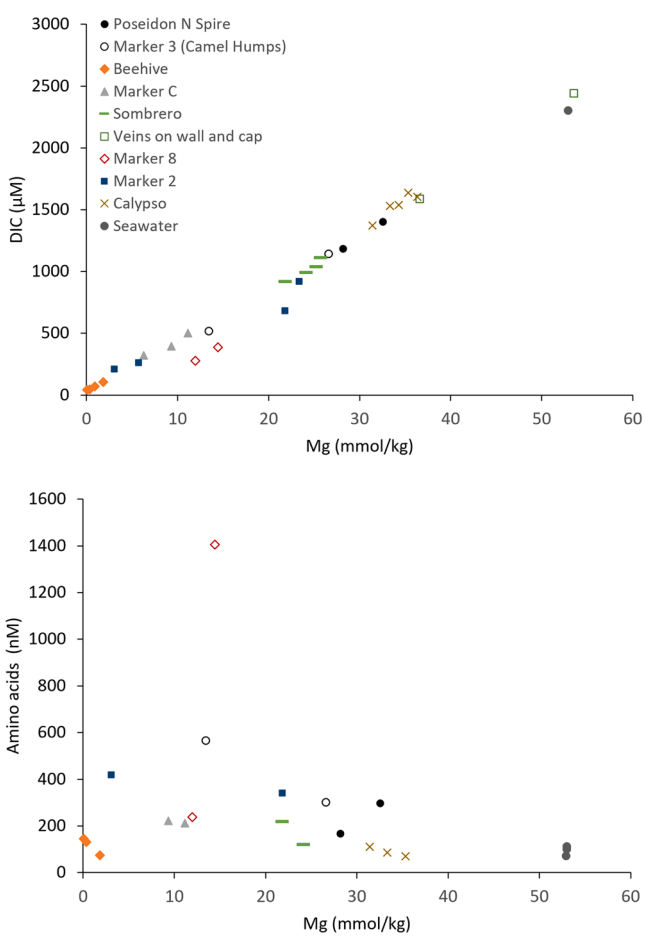

Fig. 2. Concentrations of (A) DIC vs Mg and (B) THAA vs Mg.

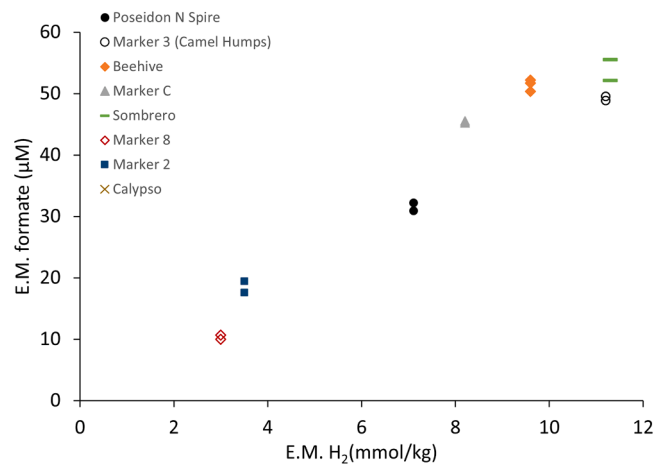

Fig. 3. Endmember formate concentrations vs endmember hydrogen concentrations.

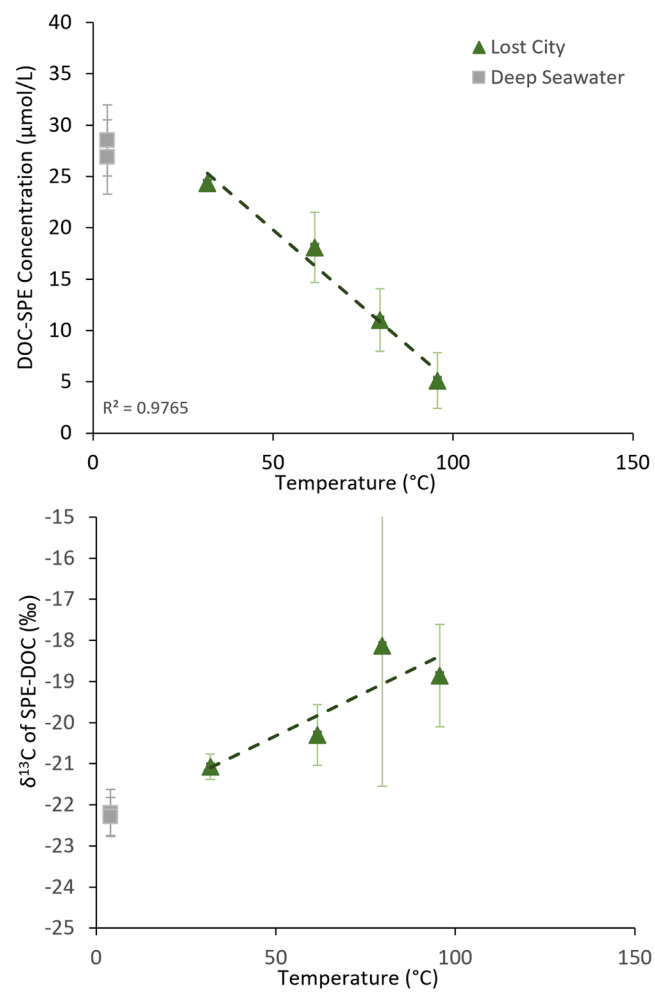

Fig. 4. Concentration (A) and isotopic composition (B) of solid phase extracts of four hydrothermal fluids and seawater. Error bars represent reproducibility of multiple analyses ($n = 3 – 5$). Dotted lines are the least squared regressions for the averaged four hydrothermal samples.

3.3. Nuclear resonance spectroscopy

The SPE extracts from deep seawater, Lost City central vents, and Lost City peripheral vents, contained two main spectral signatures in the

NMR profiles: those that have the classic broad NMR profiles associated with DOM (Lam and Simpson, 2008) and those dominated by lipid material (Fig. 5). In the spectra dominated by DOM, resonances can be assigned based on previous studies as aliphatic, carboxyl-rich alicyclic/Material Derived from Linear Terpenoids (MDLT) (Lam and Simpson, 2008; Woods et al., 2012; Arakawa et al., 2017), Carboxylic Rich Alicyclic Material (CRAM) (Hertkorn et al., 2006), and carbohydrates. In contrast, the Lost City central vents sample contains significant contributions from lipids while the DOM signal is not clearly visible. The Lost City peripheral vents sample has contributions from both the lipid input and DOM.

A more detailed analysis was carried out on the Lost City central vents sample which contains ^{1}H resonances indicative of saturated and unsaturated fatty acids. An overlay of simulated ^{1}H NMR spectra containing both saturated and unsaturated fatty acids can reproduce the spectral profile of a ^{1}H ^{1}D diffusion edited spectrum of this sample (Fig. S1). The ^{1}H diffusion edited experiment emphasizes slow diffusing components in the sample, such as large molecular weight micelles or aggregates.

Based on the profile, neither unsaturated nor saturated fatty acids alone can adequately fit the experimental ^{1}H spectral profile, indicating that this is likely a mixture of fatty acids. To further confirm our spectral assignment, the experimental and simulated 2D multiplicity edited ^{1}H–^{13}C correlation HSQC (Heteronculear Single Quantum Coherence) spectra are shown in Fig. S2. This experiment correlates ^{1}H with its directly bonded ^{13}C. These spectra display striking similarities in their spectral profiles, which indicates these fatty acids are likely the major constituents in the sample.

The integral values of each resonance are shown in the experimental 1H NMR spectrum (Fig. S1). The integral for the saturated fatty acids signal marker at 1.6 ppm is approximately 3 times that of the C = C signal marker at 5.3 ppm. After normalization for the number of protons (CH_2 for the 1.6 ppm peak and CH for 5.3 ppm peak) it can be estimated that the saturated fatty acids are at ~73% abundant vs ~27% for the unsaturated fatty acids.

It is also possible to estimate the average length of the aliphatic chains in the mixture by comparing the ratio of CH_3 (terminal groups) to $(CH_2)n$ (mid chain positions). After normalization for the number of protons, the integral ratio CH_2:CH_3 is 6.88:1. Based on a simple construct of saturated fatty acid (Fig. S1), which is composed of 1 unit of COOH : 1 unit of β-CH_2 : 1 unit of α-CH_2 : 7 units of $(-CH_2-)_n$: 1 unit of CH_3, this would give an average chain length of 11. Similar logic can be applied to estimate the average chain length of unsaturated fatty acids (Fig. S1), translating to a total average chain length of 13. Molecules with longer and shorter chain lengths are also likely present, but when all considered together have an average chain length of ~11 or 13 units.

3.4. GC/MS analysis

To confirm the results of the non-destructive NMR analysis, the SPE extracts were dried under N_2 to eliminate the deuterated methanol and analyzed by GC/MS. The major peaks that could be positively identified based on matches with external standards and the National Institute of Standards and Technology Mass Spectral library included the fatty acids decanoic acid (C10:0), dodecanoic acid (C12:0), and oleic acid (C18:1). Several additional peaks in the spectra could not be positively identified but did not have fragmentation patterns consistent with fatty acids.

3.5. Isotopic signature (^{13}C, ^{14}C) of dissolved organic carbon

The composition of DOC from seven hydrothermal fluids and one deep seawater sample were determined by UV oxidation (Table 1). The $F^{14}C$ content of the organic carbon in endmember fluids ranged from 0.030 ± 0.005 to 0.237 ± 0.005, significantly lower than deep seawater values of 0.6235 ± 0.005 while the measured $\delta^{13}C_{DOC}$ values were more positive (−10.9 to −4.1‰ vs −22‰; Fig. 6).

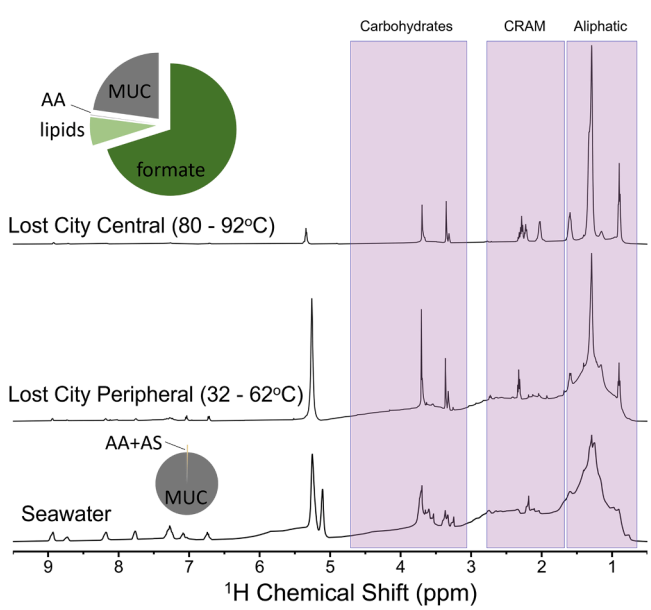

Fig. 5. ^{1}D ^{1}H NMR spectra from SPEs combined from the central vents (Beehive +C), peripheral vents (Sombrero + Calypso), and seawater (Table S2). The spectra profile of seawater and the peripheral vents where local seawater is entrained in the near subseafloor contain broad resonances indicative of heterogenous mixtures of various molecular weight compounds, and are consistent with the presence of carbohydrates, CRAM, and aliphatic material typical of deep seawater. These resonances are absent in the hottest, central Lost City sample which is instead dominated by biological signatures from lipids. Pie charts reflect the DOC composition of fluids from seawater (41.2 μM) and Beehive (73.7 μM). Most seawater is molecularly uncharacterizable (MUC) but contains small contributions of amino acids (AA) and amino sugars (AS) (Benner, 2002).

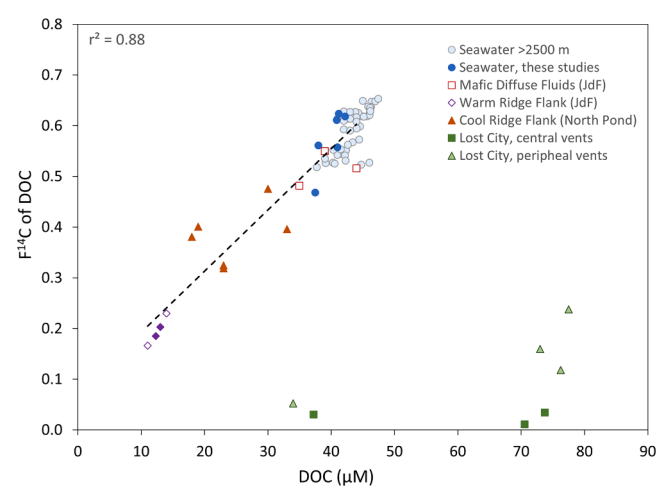

Fig. 6. $F^{14}C_{DOC}$ vs. DOC concentrations of Lost City fluids in comparison to data previously reported from mafic systems. Data sources: Lost City (this paper); Juan de Fuca fluids (JdFR; McCarthy et al., 2011; Lin et al., 2019); North Pond fluids (Walter et al., 2018). Water column data from >2500 m plotted for comparison (Druffel et al., 1992, 2015, 2016, 2021). Data from ultrafiltrated dissolved organic carbon (UDOM, >1000 Da) are denoted with hollow symbols. Dotted line is the least squares regression of the samples from mafic settings.

4. Discussion

4.1. Loss of seawater dissolved organic carbon

Several lines of evidence point to the near complete removal of seawater organics during passage through the circulation system. DOC concentrations in Lost City fluids are generally higher than seawater (58.6 ± 14.2 μM vs 41.4 ± 0.7 μM) but carry an isotopic composition that precludes the survival of seawater organics during circulation (Table 2; Fig. 1). Fluids from the center of the field (Markers C, 2, B) have isotopic signatures ($F^{14}C_{DOC}$ = 0.011 – 0.034; $\delta^{13}C_{DOC}$ = −2.9 to −5.5 ‰) indicating organics contain substantially less ^{14}C and more ^{13}C than seawater organics ($F^{14}C_{DOC}$ = 0.61 – 0.62; $\delta^{13}C_{DOC}$ = −22‰).

These data can be used to test the idea that seawater DOC survives passage through the circulation system intact. If it does, a concentration and stable carbon mass balance would be a mixture of seawater DOC and additional material from the hydrothermal system:

$$[DOC]_{EM} = [DOC]_{SWD} + [DOC]_{H} \quad (1)$$

$$[DOC]_{EM} \times R_{EM} = [DOC]_{SWD} \times R_{SWD} + [DOC]_{H} \times R_{H} \quad (2)$$

Where [DOC] is the concentration and R is the stable carbon isotopic ratio of the sampled endmember fluid (EM), seawater derived organics (SWD), and hydrothermal organics (H). Assuming seawater DOC (41 μM, −22.2 ‰) is present unaltered in the endmember fluids measured at Marker C (70.6 μM, −4.6 ‰) and Marker B (73.7 μM, −5.5 ‰), approximately 30 μM of hydrothermally sourced DOC with a $\delta^{13}C_{DOC}$ signature of +20‰ would need to be added. In addition, the $F^{14}C$ of these endmembers are equivalent to seawater that has aged by ~35,000 years. These constraints are difficult to reconcile with previous observations that the vast majority of Lost City organics have $\delta^{13}C$ values < 0 ‰ (Lang et al., 2018) and data from short-lived radioisotopes that suggest fluid residence times of < 3 years (Moore et al., 2021). Furthermore, endmember Marker 2 fluids have DOC concentrations lower than seawater (37.5 vs 41.4 ± 0.7 μM) with a substantially more positive $\delta^{13}C$ value (−2.9 ‰) making a concentration and ^{13}C isotopic mass balance impossible to resolve if seawater DOC is unaltered during circulation.

With the conservative assumption that all newly synthesized organics lack radiocarbon, the $F^{14}C$ signatures from Markers C, 2, and Beehive can instead be used to constrain the maximum contribution of seawater-derived organics present in pure, endmember fluids. If the DOC in endmember fluids is a mixture of the DOC that remains from downwelling seawater and ^{14}C-free organics, the sampled fluids are represented as:

$$[DOC]_{EM} \times F^{14}C_{EM} = [DOC]_{SWD} \times F^{14}C_{SWD} + [DOC]_{H} \times F^{14}C_{H} \quad (3)$$

where the designations are the same as the ^{13}C mass balance equation and $F^{14}C$ is the radiocarbon signature of each. After correcting for the entrainment of seawater during sampling, fluids from the Marker C vent contain 70.6 μM with a $F^{14}C$ of 0.011 ± 0.005 (Table 1). Local seawater has a $F^{14}C_{SWD}$ of 0.6235 ± 0.005 while the $F^{14}C_{H}$ of ^{14}C-free carbon will be 0. Solving for $[DOC]_{SWD}$ gives a value of 1.2 ± 0.6 μM. At Markers 2 and Beehive the same approach results in a $[DOC]_{SWD}$ of 1.8 ± 0.3 μM and 4.0 ± 0.4 μM, respectively. Compared to local deep seawater concentrations of 41.2 μM, up to 97% of seawater DOC has been stripped from the fluids. Any modern ^{14}C incorporated into the hydrothermal organics would increase the calculated amount of seawater stripped from the DOC.

Fluids from the peripheral of the field (Markers 8, Sombrero) and from central vent Marker 3 contain more ^{14}C in the DOC pool than those from Markers C, 2, and Beehive (Table 1). Seawater is entrained in the near subsurface at Markers 8, Sombrero, and 3 (Lowell, 2017; Aquino et al., 2022), allowing the incorporation of modern, seawater-derived ^{14}C into organic compounds. Hydrothermal fluids at Lost City have vanishingly low concentrations of DIC so when seawater is entrained (Fig. 2), formate rapidly equilibrates with the inorganic carbon pool, driving the $F^{14}C$ of formate to more modern values (Lang et al., 2018), and adding ^{14}C to the bulk DOC pool. This seawater-derived ^{14}C is also incorporated into biological biomass (Lang et al., 2012), and would transfer into dissolved organics through typical degradative processes.

The fraction of organics that can be isolated by SPE is also consistent with the loss of RDOC in the hydrothermal fluids. SPE preferentially isolates higher molecular weight and less polar compounds but does not recover small, polar organics such as formate and acetate (Hawkes et al., 2015; Johnson et al., 2017). Deep seawater contains complex mixture of organic molecules, but has very little contributions from the small, polar compounds that contribute most of the carbon in Lost City fluids. The hottest fluids contain 81% less SPE-DOC than local seawater, reflecting the loss of the larger, more complex, less polar material present in deep seawater despite bulk DOC concentrations that are similar or higher. It is also more enriched in ^{13}C (Table 3; Fig. S1; Table S2), consistent with the trend in the bulk DOC pool.

Finally, the NMR spectra of organics isolated by SPE confirm that the organic components commonly found in seawater are absent in Lost City fluids. Deep seawater DOM is dominated by carboxylic rich alicyclic material (CRAM) and carbohydrates (Hertkorn et al., 2006; Arakawa et al., 2017). These resonances are absent in the hottest fluids from Lost City (Fig. 5).

4.2. Removal rates of DOC

The removal of DOC must occur rapidly in the Lost City system, as the residence time of fluid circulation is short, less than 3 years (Moore et al., 2021). The removal of 40 μM of seawater-derived DOC during circulation translates to a removal rate of 13 μmol C L^{-1} y^{-1}. By comparison, in the cool mafic crustal lithosphere DOC is removed at a rate of 0.02 – 0.008 μmol C L^{-1} y^{-1} at North Pond (Shah Walter et al., 2018) and 0.002 – 0.003 μmol C L^{-1} y^{-1} on the Juan de Fuca ridge (Lin et al., 2012), or 665 – 1650 times more slowly. The removal rate at Lost City is twice as rapid than even mafic high temperature black smoker systems that have similar residence times (< 3 y; (Kadko and Moore, 1988)) but smaller total losses of DOC (20 μM; (Lang et al., 2006; Longnecker et al., 2018)) resulting in a removal of ~7 μmol C L^{-1} y^{-1}.

4.3. Composition and isotopic signature of organics exported to the deep sea

Instead of the long-lived refractory organic matter that dominates seawater, Lost City fluids contain freshly produced ^{14}C-free organic matter synthesized from abiotic and biological processes. Formate (BDL-52 μM) positively co-varies with hydrogen concentrations (Fig. 3), reflecting its rapid equilibration. Based on its ^{13}C and ^{14}C content, formate is likely formed through a combination of abiotic synthesis in the deep subsurface from ^{14}C-free CO_2 and in the near subsurface from microbial equilibration with seawater DIC (Lang et al., 2010, 2018). The lower DOC at Marker 2 can be largely attributed to lower formate abundances. The more negative $\delta^{13}C_{DIC}$ at this site likely reflects, in part, the conversion of formate into DIC. In the main field, acetate (0 – 6.2 μM) was detected in only minor amounts in the fluids. In fluids from the Beehive vent, these semi-volatile compounds contribute 70% of the total DOC. Hydrolizable amino acids range from 70 – 566 nM in fluids from the main field. At Beehive, they contribute <1% of the total DOC.

A detailed NMR analysis of the hottest fluids indicate the presence of saturated and unsaturated fatty acids with an average chain length of 11 - 13 (Section 3.3). The presence of these compounds was confirmed by GC/MS (Section 3.4). Previous work has also indicated the presence of C8-C18 fatty acids in the fluids (Konn et al., 2015; McCollom et al., 2015). The microbial communities inhabiting the chimneys produce saturated and unsaturated fatty acids, dominated by C16 and C18 chain lengths (Bradley et al., 2009). The shorter chain molecules identified in

the fluids may be due to their preferential mobilization into hot fluids (McCollom et al., 2015; Simoneit et al., 1988), making biological sources the most likely source of these compounds. In short, the 5.1 ± 2.7 μmol C/L present as SPE-DOC in Beehive fluids, or 6.9% of the DOC, can be largely attributed to lipids.

The picture that emerges from these data is that during circulation, long-lived refractory organic matter is rapidly stripped from the deep seawater and replaced by small, polar organic compounds that can be readily utilized by microbial populations. These processes may occur at different points of the circulation pathway. For example, the removal of seawater DOC may occur in the more altered, clay-rich portion of the downwelling limb of the recharge pathway (see Section 4.5). The addition of small polar compounds may occur when fluids are deeper in the system, when they are hotter and contain abundant H_2, making abiotic organic synthesis reactions more favorable. Biologically derived lipids and amino acids are most likely added as the fluids pass ascend through the carbonate chimneys that contain dense biofilms. A total of 77% of the DOC from the Beehive vent fluids can be accounted for at the molecular level, in stark contrast to most deep ocean settings where <5% of DOC molecularly uncharacterizable (Benner, 2002).

4.4. Implications for the modern and ancient oceanic carbon cycle

While the amount of organics lost per liter of fluid is substantially larger than in cool mafic systems, the global flux of organic carbon out of and into the ocean is likely smaller due to a smaller water flux though ultramafic environments. The water flux passing through hydrothermal systems influenced by serpentinization is less well constrained than mafic environments, but has been estimated as 6×10^{13} kg seawater per year (Keir, 2010). At Lost City, a liter of downwelling seawater is stripped of up to 41 μM of recalcitrant DOC, and gains 35–75 μM of ^{14}C-depleted, labile DOC. If these conditions are similar in ultramafic other systems, it would translate to a total loss of 2.8×10^{10} g C of refractory seawater DOC, in conjunction with a gain of $2.4 – 5.3 \times 10^{10}$ g C of pre-aged DOC.

The bulk DOC loss is similar to high temperature mafic-hosted hydrothermal systems ($0.7 – 1.4 \times 10^{10}$ g C $y^{-1;}$ (Lang et al., 2006)) but smaller than the removal of DOC in cool ridge flank environments ($9 – 14 \times 10^{11}$ g C $y^{-1;}$ (Shah Walter et al., 2018)) due to the large water flux through those systems. While mafic systems may allow the continued survival of the most refractory and long-lived portion of the DOC pool (Lin et al., 2019), it appears to be nearly completely removed in the Lost City system.

4.5. Potential mechanisms of DOC removal

The more extensive and rapid removal of refractory DOC at Lost City than other locations provides insights into the mechanism of loss. In hydrothermal systems, DOC can be oxidized to inorganic carbon via thermal degradation or microbial heterotrophy, or sorbed onto mineral surfaces. While all processes likely happen to some extent in all systems, the more extensive and rapid removal of DOC at Lost City than in mafic environments suggests a control that is unique to these environments.

Black smoker mafic systems reach temperatures >300 °C, while the highest temperature that Lost City fluids reach is ~180 – 250 °C (Proskurowski et al., 2006; Lang et al., 2012;Seyfried et al., 2015). Rocks recovered from the subseafloor of the Atlantis Massif have carbonates veins with low δ^{13}C values (down to −12.5 ‰) that could be formed from seawater DOC that is oxidized to CO_2 then deposited as calcium carbonate (Ternieten et al., 2021). While thermal degradation is likely the cause of a portion of DOC removal, the residence times of fluids passing through ultramafic and black smoker systems are similar, while the loss of seawater organics is more extensive at Lost City, suggesting that thermal breakdown is not the primary cause for the difference.

Microbial heterotrophs have been identified in mafic and ultramafic crustal environments, and likely play an important role in controlling the concentration and composition of fluid organics in many hydrothermal settings. As discussed above, however, the heterotrophic removal of DOC in cool mafic crust occurs at a rate >650 times slower than the losses observed at Lost City. When combined with the extremely low abundances of microbial populations recovered from subseafloor rocks at the Atlantis Massif (Früh-Green et al., 2018), more extensive heterotrophy is also unlikely to be the cause of more extensive RDOC removal during circulation through the Lost City system.

Mineralogy is the most fundamental difference between mafic and ultramafic environments, and has the potential to lead to different outcomes for organic matter. The sorption of organic molecules onto mineral surfaces is an important process in ocean sediments, water column particulates, and soils (Hedges and Keil, 1995; Wagai and Mayer, 2007; LaRowe et al., 2017). Iron oxides and clays bind organic carbon and preserve compounds for millennia (Lalonde et al., 2012; Hemingway et al., 2019). Clay minerals are a common alteration phase in both mafic and ultramafic rocks, particularly in low temperature alteration zones (<100 °C; MacDonald and Fyfe, 1985; Schwarzenbach and Harris, 2023) as is magnetite, a mineral primarily composed of iron oxide (Frost and Beard, 2007; Rouméjon et al., 2018). Organic compounds identified in ultramafic rocks including the aromatic amino acid tryptophan and condensed carbonaceous matter are physically associated with iron-rich serpentine, iron-rich saponite clays, and iron oxides (Ménez et al., 2018; Sforna et al., 2018; Andreani and Ménez, 2019; Nan et al., 2021). Clays and iron oxides are also a common alteration phase of the basalts and gabbros that comprise mafic systems, particularly in older, low temperature ridge flank systems (Schwarzenbach and Harris, 2023). Iron-rich serpentine, in contrast, is an alteration phase common in ultramafic, but not mafic, systems. Differences in minerology between mafic and ultramafic environments are one potential mechanism that could lead to more extensive sequestration of seawater organics and account for the different extents and rates of DOC removal.

4.6. Implications for interpreting organic signatures in crustal rocks

Oceanic peridotites contain up to 1500 ppm of organic carbon in comparison to up to 300 ppm of in gabbros from slow- and ultra-slow spreading ridges ((Früh-Green et al., 2004) and references therein). The presence of organic molecules in these rocks could be attributed to abiotic synthesis (Ménez et al., 2018; Sforna et al., 2018), subseafloor biological activity (Ménez et al., 2012; Motamedi et al., 2020; Goordial et al., 2021), and/or deposition of seawater DOC (Delacour et al., 2008; Ternieten et al., 2021).

Our observation that seawater DOC is stripped from circulating fluids supports the interpretation that it constitutes a significant portion of the total organic carbon found in oceanic peridotites (Delacour et al., 2008; Ternieten et al., 2021). Non-carbonate carbon in rocks from the Atlantis Massif have δ^{13}C values (−28 to −20‰) that coincide in part with the isotopic signature of seawater DOC, and contain compounds consistent with a seawater-derived source (Delacour et al., 2008; Ternieten et al., 2021). Peridotites at the Atlantis Massif and elsewhere have undergone pervasive serpentinization under low water/rock ratios, a series of alteration reactions that results in much of the water being consumed (Romejon et al., 2018). Logically, any organic matter carried with the seawater that hydrates the rock would remain the solid substrate. Additional seawater carbon is also deposited along later zones of high fluid flow pathways, as suggested by the higher abundances of non-carbonate carbon that is associated with carbonates (Ternieten et al., 2021). The Lost City hydrothermal system has been active for at least 120,000 years (Ludwig et al., 2011). Based on our estimates that of 2.8×10^{10} g C yr^{-1} are removed during circulation (Section 4.4), a total of $0.79 – 5.5 \times 10^{15}$ g of seawater organic carbon would have been deposited in the subsurface ultramafic rocks globally, potentially contributing to their larger organic content than mafic rocks. The rocks associated with the Lost City field were first exhumed 1.5 to 2 million years ago (Cann et al., 1997), allowing an order-of-magnitude larger

amount of reduced carbon carried with seawater to potentially be deposited.

The molecular composition of the organics identified in ultramafic rocks can provide valuable insights into their sources. The elevated temperatures in the subseafloor would cause structural modification, including breaking weaker bonds and the formation of more stable molecules (Simoneit et al., 1988) such as PAHs and saturated hydrocarbons (Rushdi and Simoneit, 2004; Simoneit, 1992). Macromolecular condensation reactions also occur under these conditions (Simoneit, 1992; Seewald et al., 2000). Studies that identify organic compounds in association with mineral-reactive surfaces, particularly those that identify aromatic compounds and condensed organic material, should consider the possibility that these molecules were derived from circulating seawater and modified by condensation and reduction reactions under subseafloor conditions.

CRediT authorship contribution statement

Susan Q. Lang: Writing – review & editing, Writing – original draft, Supervision, Resources, Project administration, Methodology, Investigation, Funding acquisition, Formal analysis, Data curation, Conceptualization. **Bryan Benitez-Nelson:** Writing – review & editing, Methodology, Formal analysis, Data curation. **Malayika Vincent:** Writing – review & editing, Methodology, Formal analysis, Data curation. **Ronald Soong:** Writing – review & editing, Writing – original draft, Formal analysis, Data curation. **Flavio V.C. Kock:** Writing – review & editing, Writing – original draft, Formal analysis, Data curation. **Daniel H. Lysak:** Writing – review & editing, Writing – original draft, Formal analysis, Data curation. **Amy Jenne:** Writing – review & editing, Writing – original draft, Formal analysis, Data curation. **André J. Simpson:** Data curation, Formal analysis, Writing – original draft, Writing – review & editing.

Declaration of competing interest

The authors declare that they have no known competing financial interests or personal relationships that could have appeared to influence the work reported in this paper.

Data availability

All data is provided in the tables and figures of the manuscript.

Acknowledgements

We thank the captain and crews of the R/V Atlantis and ROV Jason and Cameron Henderson, Jessica Frankle, and Aaron Mau for laboratory support. Funding was provided by National Science Foundation award OCE-1536702 to SQL, the Natural Sciences and Engineering Research Council of Canada (NSERC) [Alliance (ALLRP 549399) to AJS, the Alliance (ALLRP 555452) and Discovery Programs (RGPIN-2019-04165)], the Canada Foundation for Innovation (CFI), the Ontario Ministry of Research and Innovation (MRI) to AJS. FVCK would like to thank the University of Toronto for an Inclusive Excellence Postdoctoral Fellowship Award. We thank editor Dr. Laurence Coogan, reviewer Dr. Suni Shah Walter, and an anonymous reviewer, whose input greatly improved the manuscript.

Supplementary materials

Supplementary material associated with this article can be found, in the online version, at doi:10.1016/j.epsl.2024.118600.

References

Andreani, M., Menez, B., 2019. New perspectives on abiotic organic synthesis and processing during hydrothermal lithosphere. In: Orcutt, B.N., Daniel, I., Dasgupta, R. (Eds.), Deep Carbon Past to Present. Cambridge University Press, pp. 447–479.
Aquino, K.A., Fruh-Green, G.L., Rickli, J., Bernasconi, S.M., Lang, S.Q., Lilley, M.D., Butterfield, D.A., 2022. Multi-stage evolution of the Lost City hydrothermal vent fluids. Geochim. Cosmochim. Acta 332, 239–262.
Arakawa, N., Aluwihare, L.I., Simpson, A.J., Soong, R., Stephens, B.M., Lane-Coplen, D., 2017. Carotenoids are the likely precursor of a significant fraction of marine dissolved organic matter. Sci. Adv. 3 (9), e1602976.
Benner, R., 2002. Chemical composition and reactivity. In: Hansell, D.A., Carlson, C.A. (Eds.), Biogeochemistry of Marine Dissolved Organic Matter. Academic Press, pp. 59–90.
Bradley, A., Hayes, J., Summons, R., 2009. Extraordinary C-13 enrichment of diether lipids at the Lost City Hydrothermal Field indicates a carbon-limited ecosystem. Geochim. Cosmochim. Acta 73 (1), 102–118.
Cann, J.R., Blackman, D.K., Smith, D.K., McAllister, E., Janssen, B., Mello, S., Avgerinos, E., Pascoe, A.R., Escartin, J., 1997. Corrugated slip surfaces formed at ridge-transform intersections on the Mid-Atlantic Ridge. Nature 385 (6614), 329–332.
Cannat, M., Fontaine, F., Escartin, J., 2010. Serpentinization and associated hydrogen and methane flux at slow spreading ridges. In Diversity of hydrothermal systems on slow spreading ocean ridges. In: Rona, P.A., Devey, C.W., Dyment, J., Murton, B.J. (Eds.), Diversity of Hydrothermal Systems on Slow Spreading Ocean ridges: Vol. 188. American Geophysical Union.
Delacour, A., Früh-Green, G.L., Bernasconi, S.M., Schaeffer, P., Kelley, D.S., 2008. Carbon geochemistry of serpentinites in the Lost City hydrothermal system (30°N, MAR). Geochim. Cosmochim. Acta, 72 (15), 3681–3702.
Druffel, E.R.M., Griffin, S., 2015. Radiocarbon in dissolved organic carbon of the South Pacific Ocean. Geophys. Res. Lett. 42, 4096–4101.
Druffel, E.R.M., Williams, P.M., Bauer, J.E., Ertel, J.R., 1992. Cycling of dissolved and particulate organic-matter in the open ocean'. J. Geophys. Res. Oceans 97 (C10), 15639–15659.
Druffel, E.R.M., Griffin, S., Coppola, A.I., Walker, B.D., 2016. Radiocarbon in dissolved organic carbon of the Atlantic Ocean. Geophys. Res. Lett. 43 (10), 5279–5286.
Druffel, E.R.M., Griffin, S., Lewis, C.B., Rudresh, M., Garcia, N.G., Key, R.M., McNichol, A.P., Hauksson, N.E., Walker, B.D., 2021. Dissolved organic radiocarbon in the eastern pacific and southern oceans. Geophys. Res. Lett. 48 (10), e2021GL092904.
Evans, B.W., 2008. Control of the products of serpentinization by the (FeMg1)-Mg-2 exchange potential of olivine and orthopyroxene. J. Petrol. 49 (10), 1873–1887.
Foustoukos, D.I., Seyfried, W.E., 2004. Hydrocarbons in hydrothermal vent fluids: the role of chromium-bearing catalysts. Science 304 (5673), 1002–1005.
Früh-Green, G.L., Connolly, J.A.D., Plas, A., Kelley, D.S., Grobety, B., 2004. Serpentinization of oceanic peridotites: implications for geochemical cycles and biological activity. Subseafloor Biosph. Mid-Ocean Ranges 144, 119–136.
Früh-Green, G.L., Orcutt, B.N., Roumejon, S., Lilley, M.D., Morono, Y., Cotterill, C., Green, S., Escartin, J., John, B.E., McCaig, A.M., Cannat, M., Menez, B., Schwarzenbach, E.M., Williams, M.J., Morgan, S., Lang, S.Q., Schrenk, M.O., Brazelton, W.J., Akizawa, N., Boschi, C., Dunkel, K.G., Quemeneur, M., Whattam, S. A., Mayhew, L., Harris, M., Bayrakci, G., Behrmann, J.H., Herrero-Bervera, E., Hesse, K., Liu, H.Q., Ratnayake, A.S., Twing, K., Weis, D., Zhao, R., Bilenker, L., 2018. Magmatism, serpentinization and life: insights through drilling the Atlantis Massif (IODP Expedition 357). Lithos 323, 137–155.
Frost, B.R., Beard, J.S., 2007. On silica activity and serpentinization. J. Petrol. 48 (7), 1351–1368.
Goordial, J., D'Angelo, T., Labonté, J.M., Poulton, N.J., Brown, J.M., Stepanauskas, R., Fruh-Green, G.L., Orcutt, B.N., 2021. Microbial diversity and function in shallow subsurface sediment and oceanic lithosphere of the Atlantis Massif. mBio 12, e00490. -21.
Hansell, D.A., 2013. Recalcitrant dissolved organic carbon fractions. Annu. Rev. Mar. Sci. 5 (5), 421–445.
Hawkes, J.A., Rossel, P.E., Stubbins, A., Butterfield, D., Connelly, D.P., Achterberg, E.P., Koschinsky, A., Chavagnac, V., Hansen, C.T., Bach, W., Dittmar, T., 2015. Efficient removal of recalcitrant deep-ocean dissolved organic matter during hydrothermal circulation. Nat. Geosci. 8 (11), 856. -+.
Hedges, J.I., Keil, R.G., 1995. Sedimentary organic matter preservation - an assessment and speculative synthesis. Mar. Chem. 49 (2–3), 81–115.
Hemingway, J.D., Rothman, D.H., Grant, K.E., Rosengard, S.Z., Eglinton, T.I., Derry, L.A., Galy, V.V., 2019. Mineral protection regulates long-term global preservation of natural organic carbon. Nature 570 (7760), 228. -+.
Hertkorn, N., Benner, R., Frommberger, M., Schmitt-Kopplin, P., Witt, M., Kaiser, K., Kettrup, A., Hedges, J.I., 2006. Characterization of a major refractory component of marine dissolved organic matter. Geochim. Cosmochim. Acta 70 (12), 2990–3010.
Johnson, W.M., Soule, M.C.K., Kujawinski, E.B., 2017. Extraction efficiency and quantification of dissolved metabolites in targeted marine metabolomics. Limnol. Oceanogr. Methods 15 (4), 417–428.
Kadko, D., Moore, W., 1988. Radiochemical constraints on the crustal residence time of submarine hydrothermal fluids–endeavor ridge. Geochim. Cosmochim. Acta 52 (3), 659–668.
Keir, R.S., 2010. A note on the fluxes of abiogenic methane and hydrogen from mid-ocean ridges. Geophys. Res. Lett. 37, L24609.
Kelley, D.S., Karson, J.A., Früh-Green, G.L., Yoerger, D.R., Shank, T.M., Butterfield, D.A., Hayes, J.M., Schrenk, M.O., Olson, E.J., Proskurowski, G., Jakuba, M., Bradley, A., Larson, B., Ludwig, K., Glickson, D., Buckman, K., Bradley, A.S., Brazelton, W.J.,

Roe, K., Elend, M.J., Delacour, A., Bernasconi, S.M., Lilley, M.D., Baross, J.A., Summons, R.E., Sylva, S.P., 2005. A serpentinite-hosted ecosystem: the lost city hydrothermal field. Science 307, 1428–1434.
Konn, C., Charlou, J.L., Holm, N.G., Mousis, O., 2015. The production of methane, hydrogen, and organic compounds in ultramafic-hosted hydrothermal vents of the mid-atlantic ridge. Astrobiology 15 (5), 381–399.
Lalonde, K., Mucci, A., Ouellet, A., Gelinas, Y., 2012. Preservation of organic matter in sediments promoted by iron'. Nature 483 (7388), 198–200.
Lam, B., Simpson, A., 2008. Direct 1H NMR spectroscopy of dissolved organic matter in natural waters. Analyst 133 (2), 263–269.
Lang, S.Q., Butterfield, D.A., Lilley, M.D., Johnson, H.P., Hedges, J.I., 2006. Dissolved organic carbon in ridge-axis and ridge-flank hydrothermal systems. Geochim. Cosmochim. Acta 70 (15), 3830–3842.
Lang, S.Q., Butterfield, D.A., Schulte, M., Kelley, D.S., Lilley, M.D., 2010. Elevated concentrations of formate, acetate and dissolved organic carbon found at the Lost City hydrothermal field. Geochim. Cosmochim. Acta 74 (3), 941–952.
Lang, S.Q., Früh-Green, G.L., Bernasconi, S.M., Lilley, M.D., Proskurowski, G., Mehay, S., Butterfield, D.A., 2012. Microbial utilization of abiogenic carbon and hydrogen in a serpentinite-hosted system. Geochim. Cosmochim. Acta 92, 82–99.
Lang, S.Q., Früh-Green, G.L., Bernasconi, S.M., Butterfield, D.A., 2013. Sources of organic nitrogen at the serpentinite-hosted Lost City hydrothermal field. Geobiology 11 (2), 154–169.
Lang, S.Q., Früh-Green, G.L., Bernasconi, S.M., Brazelton, W.J., Schrenk, M.O., McGonigle, J.M., 2018. Deeply-sourced formate fuels sulfate reducers but not methanogens at Lost City hydrothermal field. Sci. Rep. 8, 1–10.
Lang, S.Q., 2018. Dissolved organic matter in submarine hydrothermal systems. In: Hansell, D.A., Carlson, C.A. (Eds.), Biogeochemistry of Marine Dissolved Organic Matter. Academic Press.
LaRowe, D.E., Burwicz, E., Arndt, S., Dale, A.W., Amend, J.P., 2017. Temperature and volume of global marine sediments. Geology 45 (3), 275–278.
Lin, H.T., Cowen, J.P., Olson, E.J., Amend, J.P., Lilley, M.D., 2012. Inorganic chemistry, gas compositions and dissolved organic carbon in fluids from sedimented young basaltic crust on the Juan de Fuca Ridge flanks. Geochim. Cosmochim. Acta 85, 213–227.
Lin, H.T., Repeta, D.J., Xu, L., Rappe, M.S., 2019. Dissolved organic carbon in basalt-hosted deep subseafloor fluids of the Juan de Fuca Ridge flank. Earth Planet. Sci. Lett. 513, 156–165.
Longnecker, K., Sievert, S.M., Sylva, S.P., Seewald, J.S., Kujawinski, E.B., 2018. Dissolved organic carbon compounds in deep-sea hydrothermal vent fluids from the East Pacific Rise at 9 degrees 50 ' N'. Org. Geochem. 125, 41–49.
Lowell, R.P., 2017. A fault-driven circulation model for the Lost City Hydrothermal Field. Geophys. Res. Lett. 44 (6), 2703–2709.
Ludwig, K.A., Shen, C.C., Kelley, D.S., Cheng, H., Edwards, R.L., 2011. U-Th systematics and Th-230 ages of carbonate chimneys at the Lost City Hydrothermal Field. Geochim. Cosmochim. Acta 75 (7), 1869–1888.
Méhay, S., Früh-Green, G.L., Lang, S.Q., Bernasconi, S.M., Brazelton, W.J., Schrenk, M. O., Schaeffer, P., Adam, P., 2013. Record of archaeal activity at the serpentinite-hosted Lost City Hydrothermal Field. Geobiology 11, 570–592.
Ménez, B., Pasini, V., Brunelli, D, 2012. Life in the hydrated suboceanic mantle. Nat. Geosci. 5, 133–137.
Ménez, B., Pisapia, C., Andreani, M., Jamme, F., Vanbellingen, Q.P., Brunelle, A., Richard, L., Dumas, P., Refregiers, M., 2018. Abiotic synthesis of amino acids in the recesses of the oceanic lithosphere. Nature 564 (7734), 59. -+.
MacDonald, A.H., Fyfe, W.S., 1985. Rates of serpentinization in seafloor environments. Tectonophysics 116 (1–2), 123–135.
Martin, W., Russell, M.J., 2007. On the origin of biochemistry at an alkaline hydrothermal vent. Philos. Trans. R. Soc. B Biol. Sci. 362 (1486), 1887–1925.
McCarthy, M., Beaupre, S., Walker, B., Voparil, I., Guilderson, T., Druffel, E., 2011. Chemosynthetic origin of C-14-depleted dissolved organic matter in a ridge-flank hydrothermal system. Nat. Geosci. 4 (1), 32–36.
McCollom, T.M., Seewald, J.S., 2007. Abiotic synthesis of organic compounds in deep-sea hydrothermal environments. Chem. Rev. 107 (2), 382–401.
McCollom, T.M., Seewald, J.S., German, C.R., 2015. Investigation of extractable organic compounds in deep-sea hydrothermal vent fluids along the Mid-Atlantic Ridge. Geochim. Cosmochim. Acta 156, 122–144.
McDermott, J.M., Seewald, J.S., German, C.R., Sylva, S.P., 2015. Pathways for abiotic organic synthesis at submarine hydrothermal fields. Proc. Natl. Acad. Sci. USA 112 (25), 7668–7672.
Moore, W.S., Frankle, J.D., Benitez-Nelson, C.R., Fruh-Green, G.L., Lang, S.Q., 2021. Activities of Ra-223 and Ra-226 in fluids from the lost city hydrothermal field require short fluid residence times. J. Geophys. Res. Oceans 126 (12), 1–18.
Motamedi, S., Orcutt, B.N., Fruh-Green, G.L., Twing, K.I., Pendleton, H.L., Brazelton, W. J., 2020. Microbial residents of the Atlantis Massif's shallow serpentinite subsurface. Appl. Environ. Microbiol. 81, e00346. -20.
Nan, J.B., King, H.E., Delen, G., Meirer, F., Weckhuysen, B.M., Guo, Z.X., Peng, X.T., Plumper, O., 2021. The nanogeochemistry of abiotic carbonaceous matter in serpentinites from the Yap Trench, western Pacific Ocean. Geology 49 (3), 330–334.
Proskurowski, G., Lilley, M.D., Kelley, D.S., Olson, E.J., 2006. Low temperature volatile production at the Lost City Hydrothermal Field, evidence from a stable isotope geothemometer. Chem. Geol. 229, 331–343.
Proskurowski, G., Lilley, M.D., Seewald, J.S., Fruh-Green, G.L., Olson, E.J., Lupton, J.E., Sylva, S.P., Kelley, D.S., 2008. Abiogenic hydrocarbon production at Lost City hydrothermal field. Science 319 (5863), 604–607.
Roumejon, S., Früh-Green, G.L., Orcutt, B.N., 2018. and the IODP Expedition 357 Science Party, 2018. Alteration heterogeneities in peridotites exhumed on the southern wall of the Atlantis Massif (IODP Expedition 357). J. Petrol. 59 (7), 1329–1358.
Rushdi, A.I., Simoneit, B.R.T., 2004. Condensation reactions and formation of amides, esters, and nitriles under hydrothermal conditions. Astrobiology 4 (2), 211–224.
Schwarzenbach, E.M., Harris, M., 2023. Hydrothermal alteration of the oceanic lithosphere. Treatise Geochem. 3e. https://pearl.plymouth.ac.uk/handle/10026.1/21547.
Seewald, J.S., Eglinton, L.B., Ong, Y.L., 2000. An experimental study of organic-inorganic interactions during vitrinite maturation. Geochim. Cosmochim. Acta 64 (9), 1577–1591.
Seyfried, W.E., Pester, N.J., Tutolo, B.M., Ding, K., 2015. The lost city hydrothermal system: constraints imposed by vent fluid chemistry and reaction path models on subseafloor heat and mass transfer processes. Geochim. Cosmochim. Acta 163, 59–79.
Sforna, M.C., Brunelli, D., Pisapia, C., Pasini, V., Malferrari, D., Menez, B., 2018. Abiotic formation of condensed carbonaceous matter in the hydrating oceanic crust. Nat. Commun. 9, 8.
Shah Walter, S.R., Jaekel, U., Osterholz, H., et al., 2018. Microbial decomposition of marine dissolved organic matter in cool oceanic crust. Nature Geosci 11, 334–339.
Simoneit, B.R.T., Kawka, O.E., Brault, M., 1988. Origin of gases and condensates in the Guaymas Basin hydrothermal system (Gulf of California). Chem. Geol. 71 (1–3), 169–182.
Simoneit, B.R.T., 1992. Aqueous organic geochemistry at high-temperature high-pressure. Orig. Life Evol. Biosph. 22 (1–4), 43–65.
Ternieten, L., Früh-Green, G.L., Bernasconi, S.M., 2021. Distribution and sources of carbon in serpentinized mantle peridotites at the Atlantis Massif (IODP Expedition 357). J. Geophys. Res. Solid Earth 126, e2021JB021973.
Wagai, R., Mayer, L.M., 2007. Sorptive stabilization of organic matter in soils by hydrous iron oxides. Geochim. Cosmochim. Acta 71 (1), 25–35.
Walter, S.R.S., Jaekel, U., Osterholz, H., Fisher, A.T., Huber, J.A., Pearson, A., Dittmar, T., Girguis, P.R., 2018. Microbial decomposition of marine dissolved organic matter in cool oceanic crust. Nat. Geosci. 11 (5), 334. -+.
Woods, G.C., Simpson, M.J., Simpson, A.J., 2012. Oxidized sterols as a significant component of dissolved organic matter: evidence from 2D HPLC in combination with 2D and 3D NMR spectroscopy. Water Res. 46 (10), 3398–3408.